

> REPLACE THIS LINE WITH YOUR MANUSCRIPT ID NUMBER (DOUBLE-CLICK HERE TO EDIT) <

Enhanced Leaf Area Index Estimation with CROP-DualGAN Network

Xueling Li, Yingying Dong, Yining Zhu, *Member, IEEE*, and Wenjiang Huang

Abstract—Quantitative estimation of regional leaf area index (LAI) is an important basis for large-scale crop growth monitoring and yield estimation. With the development of deep learning, theoretically, the use of neural networks can effectively improve the accuracy of LAI estimation, but sufficient training samples are often required due to a large number of network parameters. In an actual regional LAI quantitative estimation, there are only a few samples, which is difficult to train in networks. Therefore, a crop dual-learning generative adversarial network (CROP-DualGAN) was proposed in this article for data enhancement of small samples to estimate regional LAI. The method uses dual learning to generate hyperspectral reflectance and corresponding LAI, including two groups of generative adversarial networks, in which the generator is used to generate data that conforms to the distribution of the training set, and the discriminator is used to judge the true or false generated samples. The generators and discriminators are constantly optimized in the confrontation so that the distribution of generated data is closer to that of training samples. In single crop type experiments, 30 training samples with enhanced in VGG16 achieved the R^2 of cereal, maize and rape seed as 0.921, 0.990 and 0.956, and in SSSLAI-Net achieved the R^2 of cereal, maize and rape seed as 0.971, 0.991 and 0.962. In multiple crop types experiments, the result is lower than individual crop estimation, but higher than that of without enhancement. Finally, non-parametric test is used to prove that most improvement in LAI estimation is significant, and the accuracy won't decrease when improvement is not significant. In all, proposed method is universal and can effectively help benchmark models to improve regional LAI estimation accuracy with neural networks.

Index Terms—Leaf Area Index, Hyperspectral, Remote Sensing, CROP-DualGAN, data enhancement.

I. INTRODUCTION

LEAF area index (LAI) reflects crop growth as a significant biological parameter [1], thereby providing structured qualitative information to describe the conversion process between material on a vegetation canopy and energy. LAI plays an important role in the quantitative remote sensing of vegetation, ecosystem carbon cycling, vegetation productivity, energy balancing among vegetation, soil, and the atmosphere, and so on [2]. LAI is a crucial input parameter in ecological models and land surface models. It is often used as an indicator of vegetation conditions and is also

an important agricultural index for monitoring crop growth and estimating production [3]. Therefore, it is of great significance to quantitatively acquire spatiotemporally continuous regional LAI for crop growth monitoring and yield estimation [4].

Field LAI measurement methods include conventional direct measurement on the ground and remote sensing technology [5]. Because direct measurement has difficulty handling long time-series LAI observations in a large area [6], [7], and remote sensing technology provides an effective way to quickly and timely obtain regional LAI and has thus become an LAI monitoring trend [8], [9]. At present, LAI estimation methods mainly include statistical models, physical models, and data assimilation. Statistical methods, such as highly correlated statistical models, have high coefficients of determination, but poor for regional promotion [10]-[13]. Physical models face ill-posed problems due to complexity and are highly dependent on the authenticity of radiative transfer model simulations and proper model parameter initializations [14]-[16]. Data assimilation method is affected by the utilized observation variables and crop growth models. Each assimilation method has its application scope and conditions [17], [18].

Recently, with the development of machine learning, many machine learning methods have successively emerged to realize large regional LAI estimation based on parts of bands or vegetation indices [5], [19], [20]. The widely used machine learning methods for LAI estimation are artificial neural networks (ANNs), support vector machines (SVMs), random forests (RFs), ensembles of trees (ETs), regression trees (RTs), radial basis functions (RBFs), generalized regression neural networks (GRNNs), Gaussian process models (GPMs) and Deep Belief Networks (DBNs) [20]-[22]. ANNs fit well on complex, high-dimensional, and nonlinear data, and have high accuracy. SVMs similarly support high-dimensional inputs in regression models, but they need fewer training samples than ANNs. RF has high precision, high calculation speed, and robustness in parameter estimation, and it can rank variables according to their importance in LAI estimation [13], [19], [23]. Machine learning can improve the precision of estimation over that of traditional estimation methods, but it is very dependent

This work was supported by the National Key R&D Program of China “2021YFB3901303”, National Natural Science Foundation of China “42071423” and “42071320”, Alliance of International Science Organizations Grant “ANSO-CR-KP-2021-06”, and SINO-EU, Dragon 5 Proposal: Application Of Sino-Eu Optical Data Into Agronomic Models To Predict Crop Performance And To Monitor And Forecast Crop Pests And Diseases “ID 57457”. (Corresponding author: Yingying Dong)

X.L. Li is with the State Key Laboratory of Remote Sensing Science, Aerospace Information Research Institute, Chinese Academy of Sciences,

Beijing 100094, China (e-mail: lixl@aircas.ac.cn).

Y.Y. Dong and W. J. Huang are with the State Key Laboratory of Remote Sensing Science, Aerospace Information Research Institute, Chinese Academy of Sciences, Beijing 100094, China, and the University of Chinese Academy of Sciences, Beijing 100049, China (e-mail: dongyy@aircas.ac.cn; huangwj@aircas.ac.cn).

Y.N. Zhu is with the School of Mathematical Sciences, Capital Normal University, Beijing 100048, China (e-mail: ynzhu@cnu.edu.cn).

> REPLACE THIS LINE WITH YOUR MANUSCRIPT ID NUMBER (DOUBLE-CLICK HERE TO EDIT) <

on the number of measured training samples. Therefore, sufficient training samples are needed for model training, and the uncertainty of band combinations may affect the accuracy of LAI estimation [21], for which Bayesian networks are normally used to select hyperspectral bands for modeling [24], [25].

This article utilizes the self-learning characteristic of deep learning to solve the problems of machine learning in LAI estimation. We select all the hyperspectral bands reflectance as the network inputs for LAI estimation, according to a prior knowledge. Usually, neural networks need sufficient training samples [21], because many parameters are utilized (the number of parameters generally reaches 10^9). However, in actual regional LAI estimation, a few measured samples are obtained, which is difficult to train well in general neural networks. Aiming at using small samples to estimate parameters, it can be solved in two ways: one is to use Bayesian estimation with incorporating prior information to reduce severely biased estimates [26] or light-weight network to complete regression estimation [27, 28], the other is to realize data enhancement for small samples by deep learning [29, 30]. Adversarial networks can be used in computer vision to realize unsupervised dual learning in image-to-image translation [31]. Yi et al. [32], Qu et al. [33], and Omdal [34] utilized a dual generative adversarial network (DualGAN) to complete image-to-image translation. Li et al. [35] detected outliers and Prokopenko et al. [36] used an improved DualGAN to generate synthetic computed tomography images. In addition, adversarial networks have more applications [37], [38]. Thus, we consider utilizing DualGAN to realize data enhancement for small samples and then achieve the purpose of LAI estimation by benchmark models.

II. METHOD

A. CROP-DualGAN

A DualGAN is a GAN with dual learning capabilities that contains two groups of generators and discriminators. Generators are used to generate data with a distribution that is subject to the training samples distribution. Discriminators judge the true or false generated samples. Generators and discriminators can be continuously optimized during the confrontation to make the distribution of generated data much closer to that of the training samples. We aim to generate pairs of hyperspectral reflectance and LAI by the DualGAN. Original DualGAN can be modified according to research data, and called crop dual-learning generative adversarial network (CROP-DualGAN), as shown in Fig. 1. The generator for generating LAI is denoted as G_A , the generator for generating hyperspectral reflectance is denoted as G_B , and the corresponding discriminators are denoted as D_A and D_B .

The domain U contains all original hyperspectral reflectance and generated hyperspectral reflectance, and the domain V contains all original LAI and generated LAI. As shown in Fig. 1, the hyperspectral reflectance denoting $u \in U$ is translated to the domain V by G_A , and the generated LAI $G_A(u, z)$ in domain V is evaluated by D_A , where z denotes random noise. Then,

$G_A(u, z)$ is translated back to the domain U by G_B , obtaining reconstructed hyperspectral reflectance called $G_B(G_A(u, z), z')$, where z' denotes random noise as well. Similarly, the LAI denoting $v \in V$ is translated as generated reconstructed hyperspectral called $G_B(v, z')$ in domain U , and then $G_B(v, z')$ is translated back as reconstructed LAI called $G_A(G_B(v, z'), z)$ in domain V . D_A is trained with v and $G_A(u, z)$ as positive samples and negative examples, separately. While D_B is trained with u as positive samples, and $G_B(v, z')$ as negative samples. G_A and G_B are optimized by blinding the corresponding D_A and D_B and minimize the two reconstruction losses.

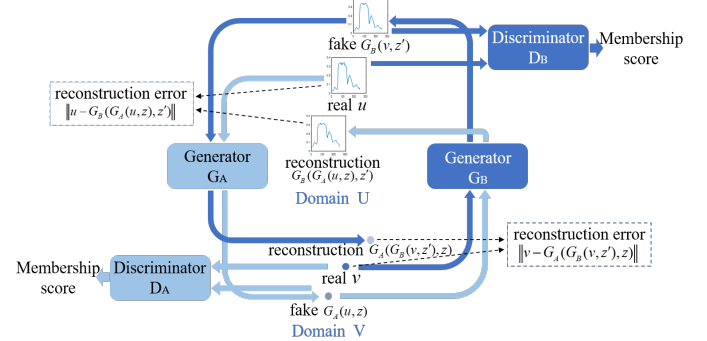


Fig. 1. Network architecture and data flow chart of CROP-DualGAN for hyperspectral reflectance and LAI translation.

G_A is a network for generating LAI according to hyperspectral reflectance, and the network contains seven basic residual blocks. The structure of the G_A network is shown in Fig. 2(a). In the basic residual blocks, the main path stacks two convolution layers with one-dimensional convolution kernel sizes as 3. Furthermore, the padding is set to the same values, and all convolution layers are activated by a rectified linear unit (ReLU). Two shortcut cases can be described as below. One is that when the numbers of channels in the main path and shortcut are different, we need a one-dimensional convolution with its kernel size as 1 to make the number of channels in the shortcut equal to that of main path (the residual block is shown in Fig. 2(b)). The other is that when the numbers of channels are the same, the shortcut's value is the output of the last residual block (the residual block is shown in Fig. 2(c)). The features learned by the residual block are obtained by adding the values of the main path and shortcut. Then, the mentioned features activated by the ReLU are the final outputs of this residual block. The outputs are used as the inputs of the maximum pooling layer for down sampling. The maximum pooling can reduce dimension and remove redundant information whose size is set to 2 normally and step size is consistent with it [39]. Padding size is set to 1 to fill the boundary, and other parameters setting to 0 represent default.

G_B is a network for generating hyperspectral reflectance according to LAI, where the inputs are LAI and the outputs are hyperspectral reflectance with 244 bands. The generation procedure is a process of mapping from low-dimensional data to high-dimensional data. The structure of the G_B network is shown in Fig. 3. The first layer of G_B is a fully connected layer with 16 neurons, meaning that the LAI values are mapped to 16-dimensional vectors. Then, the network repeats

> REPLACE THIS LINE WITH YOUR MANUSCRIPT ID NUMBER (DOUBLE-CLICK HERE TO EDIT) <

deconvolution and convolution operations, finally obtaining hyperspectral reflectance at the output layer. G_B is stimulated by the fusion of decoded features and encoded features in U-Net [39]. However, it does not utilize channel stitching to fuse features. It adds only the convolutional features in G_A to the corresponding deconvolution features in G_B . The prerequisite is

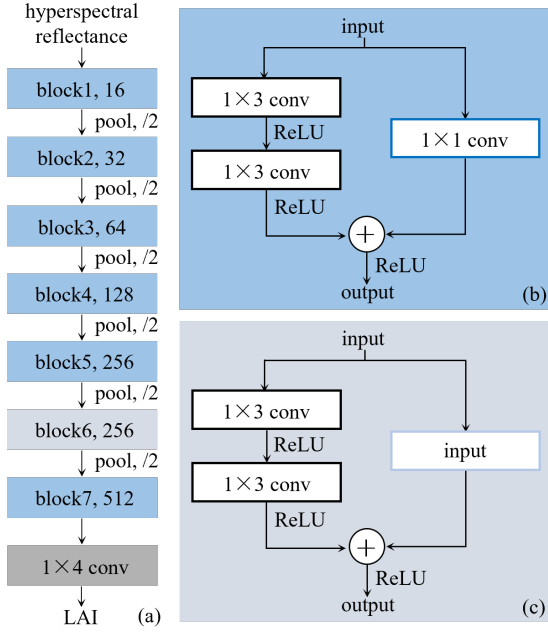


Fig. 2. G_A network for generating LAI. (a) is G_A network. (b) is network of the block1, block2, block3, block4, block5 and block7. (c) is the network of the block6.

that the dimensions of the features in the convolution step and the corresponding up sampling step are the same. And when they are different, the features with higher dimensions need to be center cropped. The features extracted by deconvolution possess only one dimension more than the features extracted by convolution, so we remove the last one-dimensional feature. In short, G_B repeats deconvolution, feature fusion and convolution operations to obtain more reliable hyperspectral reflectance. The size of the one-dimensional deconvolution kernel is 2, which is the step size. The size of the one-dimensional convolution kernel is 3, the step size is set to 1, and padding is the same as above.

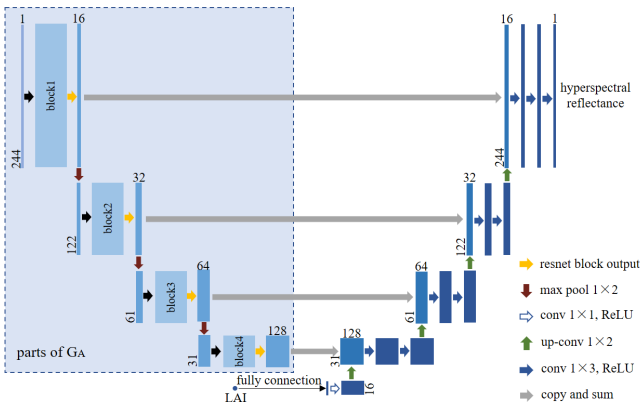


Fig. 3. G_B network for generating hyperspectral reflectance.

The D_A is a fully connected network with four layers activated by LeakyReLU (its constant λ is set to 0.2). In D_A , the numbers of neurons in the order layers are 512, 256, 128, and 1. The input of D_A is hyperspectral reflectance, and its output is a probability that discriminates generated data from real data. D_B is slightly different from D_A , which has three fully connected layers with 16, 16, and 1 neuron.

B. Loss Functions

The loss functions of G_A and G_B are optimized simultaneously, and their optimizations are related to minimized reconstruction errors.

$$l^g(u, v) = \lambda_U \|u - G_B(G_A(u, z), z')\| + \lambda_V \|v - G_A(G_B(v, z'), z)\| - D_A(G_B(u, z')) - D_B(G_A(u, z)) \quad (1)$$

Where $\|u - G_B(G_A(u, z), z')\|$ and $\|v - G_A(G_B(v, z'), z)\|$ are two reconstruction losses, and λ_U and λ_V are two constants parameters. In our study, they are equal to 5.

The loss functions of D_A and D_B are optimized respectively. They all add gradient penalties to the initial discriminator loss functions of the GAN [40]. The reason for this setting is that if the discriminators are optimal during training, the generators will encounter gradient disappearance problems and lack diversity. Based on previous research and summaries [41]-[43], the above problems can be prevented by adding gradient penalties. D_A and D_B can be defined as:

$$l_A^d(u, v) = D_A(G_A(u, z)) - D_A(v) + \lambda E_{\hat{x} \in \hat{V}} [\|\nabla_{\hat{x}} D_A(\hat{x})\|_p - 1]^2 \quad (2)$$

$$l_B^d(u, v) = D_B(G_B(u, z')) - D_B(u) + \lambda E_{x \in \hat{U}} [\|\nabla_x D_B(x)\|_p - 1]^2 \quad (3)$$

where λ is a gradient penalty constant, ∇ , E and $\|\cdot\|_p$ represent gradient, mathematical expectation and p -norm, respectively. Here, $\lambda = 10$ and $p = 2$. \hat{x} in \hat{V} and x in \hat{U} are defined as:

$$\hat{x} = \varepsilon v + (1 - \varepsilon)G_A(u, z) \quad (4)$$

$$x = \varepsilon u + (1 - \varepsilon)G_B(v, z') \quad (5)$$

where $\varepsilon \in [0, 1]$.

C. Hyperparameter Settings

We utilize the root mean squared propagation (RMSProp) algorithm to optimize the loss functions. But the choice of hyper-parameters is always a challenge, so we take a try and trail way to manually search for optimal parameters in a scope. The hyperparameters of RMSProp in D_A and D_B are set as follows. β_2 is 0.99, and the weight decay is 0.9. They are set to 0.95 and 0.9 in G_A and G_B , respectively. In addition, we provide a series of settings. For example, the initial weights are subject to a Gaussian distribution with a mean value as 0 and a standard deviation as $\sqrt{2/n}$ (where n is the number of weights in every layer) [44]. All biases are 0, the learning rate η is 2×10^{-4} , and the batch size is 4.

D. Training

The generators and discriminators alternately update in the

> REPLACE THIS LINE WITH YOUR MANUSCRIPT ID NUMBER (DOUBLE-CLICK HERE TO EDIT) <

networks. When generators G_A and G_B are fixed, discriminators D_A and D_B are trained. D_A is optimized by correctly discriminating v as true while $G_A(u, z)$ is false. Similarly, D_B is optimized by correctly discriminating u as true while $G_B(v, z')$ is fake. Similarly, when discriminators D_A and D_B are fixed, G_A and G_B are trained. G_A and G_B are optimized simultaneously to emulate “fake” outputs to blind the corresponding discriminators. To get better generators, we train the discriminators for 1 step and generators for 5 steps. The network tends to be stable as losses are within a certain range.

E. Enhanced Data Selection

Due to DualGAN is an unsupervised dual learning network for image-to-image translation, the generators G_A and G_B are structured by U-Net. Discriminators can contain fully connected layers or add additional convolution layers appropriately [31]. The outputs in discriminators evaluate the similarity between fake data and true data. When training is finished, many generated data can be obtained. Generally, images with precisely aligned pixel features in domains U and V are screened by humans [32], which is a subjective process.

For solving the problems of existing data screening methods, and ensuring that the distribution of select generated samples is much closer to the training samples distribution, we propose a more objective and reasonable method to select samples generated. According to the training samples written by $X = x_1, x_2, \dots, x_n$, the generated samples are divided into n sets written by $G_{x_1} = x_{11}, x_{12}, \dots, x_{1n_1}$, $G_{x_2} = x_{21}, x_{22}, \dots, x_{2n_2}, \dots$, and $G_{x_n} = x_{n1}, x_{n2}, \dots, x_{nn_n}$. $G_{x_1}, G_{x_2}, \dots, G_{x_n}$ are sorted by errors from small to large, separately. Then, $G'_{x_1} = x'_{11}, x'_{12}, \dots, x'_{1n_1}$, $G'_{x_2} = x'_{21}, x'_{22}, \dots, x'_{2n_2}, \dots$, and $G'_{x_n} = x'_{n1}, x'_{n2}, \dots, x'_{nn_n}$ are obtained. Finally, selected the generated samples from $G'_{x_1}, G'_{x_2}, \dots, G'_{x_n}$ in turn, combined with initial training samples to estimate LAI.

III. EXPERIMENTS

A. Experimental Flow

CROP-DualGAN realizes data enhancement for the initial training samples. Then, generated samples selected by proposed rules with initial training samples to estimate LAI based on benchmark models. Finally, the LAI estimation in this article is compared with the result of without enhancement and random selection.

B. Experimental Data

EnMAP data, including hyperspectral reflectance and LAI products, are openly published by the European Space Agency (<http://www.enmap.org/>). The research area is located in the alpine foothills of Germany (48.0514° N, 111.0760° E), and obtained on July 22, 2006. It shows cereal, maize, and rape seed in the middle and late growth stages. Atmospherically corrected [45] hyperspectral reflectance has 244 bands in the range of 420-2460 nm, where the spatial resolution is 30 meters. The LAI products are obtained by the inverse process of the coupled soil-leaf-canopy model [46].

C. Preprocessing

In the EnMAP data, the range of the original hyperspectral reflectance is within 10000, and the LAI range is from 0 to 7. Here are two ways in data preprocessing. One is that hyperspectral reflectance needs to be reduced by 1000 times, while original LAI need not be preprocessed for CROP-DualGAN to enhance samples. The other way is that generated hyperspectral reflectance needs to be reduced by 10 times for benchmark models estimation, and the original hyperspectral reflectance needs to be reduced by 10000 times. The normalization of the generated LAI and original LAI is defined by Eq. (6):

$$y = \frac{\text{LAI} - \text{LAI}_{\min}}{\text{LAI}_{\max} - \text{LAI}_{\min}} \quad (6)$$

where y is the normalized LAI.

Then, the preprocessed samples are put into the LAI estimation benchmark models for training.

D. Benchmark Models

Original training samples with selected enhanced data are put into benchmark models to estimate the LAI. In this article, Visual Geometry Group 16 (VGG16) [47] and Small Samples Learning LAI-Net (SLLAI-Net) [27] are regarded as the benchmark models to estimate LAI. Due to VGG16 and SLLAI-Net represent two different types of networks, where VGG16 with many parameters is a general classical regression network for estimation which can be applied to the research of manuscript and SLLAI-Net is a light-weight neural network which is dedicated to LAI estimation supporting small samples training.

VGG16 consists 16 weight layers, including 13 convolution layers and 3 fully connected layers. In addition, VGG16 has 5 pooling layers without weights. In the convolution layers, the one-dimensional convolution kernel size is 3, and the feature dimensions remain unchanged after the convolution layers. In the pooling layers, the pool size and step size of one-dimensional pooling are set to 2. In the fully connected layers, the numbers of neurons in the three layers with dropout are 512, 512, and 1. The initialization weights of VGG16 are subject to a Gaussian distribution with the mean value as 0 and standard deviation as $\sqrt{2/n}$ (where n is the number of weights in every layer). The learning rate η is 0.0001.

SLLAI-Net is a light-weight neural network containing two convolution layers, one pooling layer, and three fully connected layers. The kernel size and step size of the one-dimensional convolution are both 3. The numbers of channels in the first and second convolution layers are 4 and 16, respectively. The maximum pooling layer is connected after the second convolution layer, whose pooling size and step size are 3. The fully connected layers possess 32, 8, and 1 neuron. In addition, the first connection layer sets the dropout. Similar to VGG16, the initialization weights of SLLAI-Net are also subject to a Gaussian distribution with the mean value as 0 and standard deviation as $\sqrt{2/n}$. Its initial learning rate η is 0.01, which decreases with iterations increasing.

> REPLACE THIS LINE WITH YOUR MANUSCRIPT ID NUMBER (DOUBLE-CLICK HERE TO EDIT) <

E. Results

Two experiments are presented in this section. One is that 200, 100, 50, and 30 initial training samples are selected randomly according to the proportion of cereal 66.6%, maize 15.6%, and rape seed 17.8%, separately, and enhanced to 500 by CROP-DualGAN and proposed selection method. Similarly, the other is that 300 and 200 initial training samples are selected randomly according to the proportion of three kinds of crops, and enhanced to 1000. After training, the test accuracy in this article is compared with the accuracy of without enhancement and random selection. To avoid accidental results, every experiment is repeated 10 times, and average value was taken as final accuracy, standard deviation as measure of stability. Finally, Kruskal-Wallis H Test belonging to non-parametric test is used to prove whether the improvement in LAI estimation is significant.

TABLE I
COMPARISON RESULTS OF THE R² IN VGG16 (MEAN ± STANDARD DEVIATION)

Category	30			50		
	VGG16	Random -VGG16	CROP-DualGAN -VGG16	VGG16	Random -VGG16	CROP-DualGAN -VGG16
Cereal	0.840 ±0.039	0.903 ±0.046	0.921 ±0.036 <i>p</i> =0.0007	0.884 ±0.050	0.921 ±0.048	0.943 ±0.042 <i>p</i> =0.0025
Maize	0.987 ±0.006	0.987 ±0.004	0.990 ±0.004 <i>p</i> =0.0817	0.993 ±0.004	0.994 ±0.004	0.995 ±0.001 <i>p</i> =0.8197
Rape seed	0.924 ±0.021	0.939 ±0.026	0.956 ±0.010 <i>p</i> =0.0032	0.937 ±0.036	0.966 ±0.009	0.965 ±0.011 <i>p</i> =0.0319
Category	100			200		
	VGG16	Random -VGG16	CROP-DualGAN -VGG16	VGG16	Random -VGG16	CROP-DualGAN -VGG16
Cereal	0.920 ±0.021	0.931 ±0.038	0.954 ±0.014 <i>p</i> =0.0011	0.964 ±0.015	0.966 ±0.018	0.974 ±0.008 <i>p</i> =0.0692
Maize	0.996 ±0.001	0.996 ±0.002	0.997 ±0.0008 <i>p</i> =0.1004	0.998 ±0.0008	0.998 ±0.0007	0.998 ±0.0007 <i>p</i> =0.9313
Rape seed	0.963 ±0.011	0.978 ±0.006	0.979 ±0.006 <i>p</i> =0.0045	0.977 ±0.006	0.984 ±0.005	0.986 ±0.003 <i>p</i> =0.0010

Note: *p* is a value in Kruskal-Wallis H Test compared VGG16 and CROP-DualGAN-VGG16, and significance level is 0.05.

TABLE II
COMPARISON RESULTS OF THE RMSE IN VGG16 (MEAN ± STANDARD DEVIATION)

Category	30			50		
	VGG16	Random -VGG16	CROP-DualGAN -VGG16	VGG16	Random -VGG16	CROP-DualGAN -VGG16
Cereal	0.677 ±0.089	0.518 ±0.122	0.470 ±0.113 <i>p</i> =0.0012	0.573 ±0.122	0.464 ±0.146	0.394 ±0.122 <i>p</i> =0.0032
Maize	0.156 ±0.041	0.165 ±0.029	0.132 ±0.030 <i>p</i> =0.2505	0.105 ±0.038	0.108 ±0.040	0.091 ±0.015 <i>p</i> =0.6746
Rape seed	0.406 ±0.060	0.362 ±0.073	0.312 ±0.037 <i>p</i> =0.0019	0.373 ±0.115	0.280 ±0.039	0.282 ±0.053 <i>p</i> =0.0243
Category	100			200		
	VGG16	Random -VGG16	CROP-DualGAN -VGG16	VGG16	Random -VGG16	CROP-DualGAN -VGG16
Cereal	0.464 ±0.063	0.424 ±0.114	0.360 ±0.052 <i>p</i> =0.0019	0.310 ±0.077	0.295 ±0.084	0.270 ±0.040 <i>p</i> =0.0342
Maize	0.080 ±0.011	0.085 ±0.019	0.077 ±0.008 <i>p</i> =0.5432	0.063 ±0.010	0.062 ±0.009	0.064 ±0.010 <i>p</i> =0.8201
Rape seed	0.278 ±0.042	0.218 ±0.031	0.216 ±0.047 <i>p</i> =0.0155	0.223 ±0.028	0.186 ±0.026	0.176 ±0.020 <i>p</i> =0.0013

Note: *p* is a value in Kruskal-Wallis H Test compared VGG16 with CROP-DualGAN-VGG16, and significance level is 0.05.

In the single crop type experiments, Table I and Table II list the R² and RMSE of VGG16, separately. Similarly, Table III and Table IV list those of SLLAI-Net. It can be seen that proposed method achieves higher accuracy and more stable in both VGG16 and SLLAI-Net, most improvement in LAI estimation is significant, and the accuracy won't decrease when improvement is not significant. For Table I and Table II, it is clear that cereal and rape seed with 30, 50, and 100 initial training samples show that the accuracy of estimation is improved significantly with data enhancement (*p*-value is smaller than 0.05). While the results of cereal with 200 initial training samples are not significant, but won't be lower than VGG16. Maize in CROP-DualGAN-VGG16 is not significant because these have performed well in VGG16, resulting in limited improvement, but the accuracy of LAI estimation in CROP-DualGAN-VGG16 won't be lower than that of VGG16, too. Similarly, for Table III and Table IV, cereal and maize with 30, 50, and 100 initial training samples, and rape seed with 30, 50, 100 and 200 initial training samples show that the accuracy of estimation is improved significantly based on CROP-DualGAN-SLLAI (*p*-value is smaller than 0.05). While the results of cereal and maize with 200 initial training samples are not significant, because SLLAI-Net is a light-weight network supporting small samples training, and the R² of cereal and maize has achieved 0.989 and 0.995, resulting in limited improvement, but the accuracy of LAI estimation in CROP-DualGAN-SLLAI is still higher than that of SLLAI-Net.

TABLE III
COMPARISON RESULTS OF THE R² IN SLLAI-NET (MEAN ± STANDARD DEVIATION)

Category	30			50		
	SLLAI	Random -SLLAI	CROP-DualGAN -SLLAI	SLLAI	Random -SLLAI	CROP-DualGAN -SLLAI
Cereal	0.950 ±0.019	0.968 ±0.021	0.971 ±0.008 <i>p</i> =0.0140	0.969 ±0.015	0.976 ±0.011	0.982 ±0.010 <i>p</i> =0.0072
Maize	0.966 ±0.018	0.983 ±0.007	0.991 ±0.007 <i>p</i> =0.0009	0.986 ±0.006	0.992 ±0.005	0.994 ±0.005 <i>p</i> =0.0039
Rape seed	0.936 ±0.026	0.961 ±0.009	0.962 ±0.014 <i>p</i> =0.0342	0.952 ±0.019	0.971 ±0.010	0.977 ±0.006 <i>p</i> =0.0015
Category	100			200		
	SLLAI	Random -SLLAI	CROP-DualGAN -SLLAI	SLLAI	Random -SLLAI	CROP-DualGAN -SLLAI
Cereal	0.976 ±0.015	0.979 ±0.007	0.986 ±0.003 <i>p</i> =0.0267	0.989 ±0.007	0.990 ±0.007	0.992 ±0.002 <i>p</i> =0.1763
Maize	0.993 ±0.003	0.994 ±0.005	0.996 ±0.001 <i>p</i> =0.0077	0.995 ±0.003	0.996 ±0.003	0.997 ±0.002 <i>p</i> =0.1526
Rape seed	0.978 ±0.006	0.981 ±0.006	0.987 ±0.004 <i>p</i> =0.0027	0.986 ±0.004	0.983 ±0.004	0.990 ±0.002 <i>p</i> =0.0325

Note: *p* is a value in Kruskal-Wallis H Test compared SLLAI-Net with CROP-DualGAN-SLLAI, and significance level is 0.05.

In addition, SLLAI-Net is better than VGG16 for LAI estimation because that is a light-weight network for small samples training. VGG16 cannot reach the ideal accuracy in the case of small samples, but it can improve accuracy of crop estimation with the help of CROP-DualGAN. For the crop type, the accuracy of LAI estimation is related to its distribution of various crops which is shown in Fig.4. We can see that the LAI distribution of cereal, maize, and rape seed is most within LAI = 3. Besides, some LAI of cereal and rape seed are also

> REPLACE THIS LINE WITH YOUR MANUSCRIPT ID NUMBER (DOUBLE-CLICK HERE TO EDIT) <

distributed around LAI = 7, and a few between LAI = 4 and LAI = 7. Therefore, it causes data imbalance, and estimated errors mainly come from around LAI = 7. Compared with the distribution of cereal and rape seed, here are more LAI of maize distributed between LAI = 4 and LAI = 7. And fewer around LAI = 7, so the estimated accuracy of maize is higher than those of cereal and rape seed. Fig.5 and Fig.6 show the LAI estimation of VGG16 and SSSLAI-Net, respectively, based on 30 initial training samples.

TABLE IV
COMPARISON RESULTS OF THE RMSE IN SSSLAI-NET (MEAN ± STANDARD DEVIATION)

Category	30			50		
	SSLAI	Random -SSLAI	CROP-DualGAN -SSLAI	SSLAI	Random -SSLAI	CROP-DualGAN -SSLAI
Cereal	0.362 ±0.071	0.297 ±0.078	0.290 ±0.053	0.287 ±0.061	0.264 ±0.056	0.223 ±0.050
Maize	0.244 ±0.073	0.183 ±0.043	0.131 ±0.052	0.156 ±0.034	0.118 ±0.054	0.106 ±0.049
Rape seed	0.377 ±0.094	0.293 ±0.039	0.288 ±0.061	0.325 ±0.077	0.272 ±0.073	0.229 ±0.040
Category	100			200		
	SSLAI	Random -SSLAI	CROP-DualGAN -SSLAI	SSLAI	Random -SSLAI	CROP-DualGAN -SSLAI
Cereal	0.248 ±0.077	0.239 ±0.038	0.198 ±0.019	0.167 ±0.044	0.162 ±0.049	0.147 ±0.017
Maize	0.106 ±0.025	0.098 ±0.033	0.080 ±0.013	0.085 ±0.032	0.074 ±0.028	0.063 ±0.026
Rape seed	0.218 ±0.025	0.210 ±0.044	0.169 ±0.025	0.170 ±0.027	0.190 ±0.024	0.146 ±0.018

Note: p is a value in Kruskal-Wallis H Test compared SSSLAI-Net with CROP-DualGAN-SSLAI, and significance level is 0.05.

In the multiple crop types experiments, Table V and Table VI list the R^2 and RMSE obtained for three kinds of crops, respectively. Compared with single crop type experiments, the accuracy of rape seed together with cereal and maize is obviously lower than individual crop estimation. Due to benchmark models estimating LAI are data-driven methods, that is learning the relationship between hyperspectral reflectance and corresponding LAI, so the accuracy of LAI estimation is affected by data distribution. As shown in Fig.4, distribution for LAI of cereal, maize and rape seed is different. Therefore, the accuracy of cereal together with maize and rape seed is lower than cereal estimation individually, so are maize and rape seed. For Table V and Table VI, the improvement of LAI estimation is significantly in CROP-DualGAN-SSLAI. In CROP-DualGAN-VGG16, cereal and rape seed with 200 initial training samples shows that the accuracy of estimation is improved significantly and maize shows the results are not significant because these have performed well in VGG16. But the accuracy of LAI estimation in CROP-DualGAN-VGG16 don't be lower than that of VGG16. Fig.7 and Fig.8 show the LAI estimation of VGG16 and SSSLAI-Net, respectively, based on 200 initial training samples.

In term of network analysis, CROP-DualGAN can help benchmark models estimate LAI more accurate, owing to its network structure consist of two pairs of generators and

corresponding discriminators. Generators are used to generate hyperspectral reflectance and LAI, while discriminators judge the true or false samples generated by itself. The generators and discriminators can be continuously optimized during the confrontation to make the distribution of the generated data closer to the distribution of training samples. Moreover, the proposed data selection ensures samples more balanced. In this paper, the Kolmogorov-Smirnov Test is used to test whether the initial training samples and the selected generated samples have the same distribution, as shown in Fig.9. It can be seen that p -value > 0.05 which is the given significance level. That is, the samples enhanced by CROP-DualGAN have the same distribution as the initial training samples, so it is the rationality of data augmentation to effective LAI estimation improvement.

TABLE V
COMPARISON RESULTS OF THE R^2 IN THE BENCHMARK MODELS (MEAN ± STANDARD DEVIATION)

Category	200			300		
	VGG16	Random -VGG16	CROP-DualGAN -VGG16	VGG16	Random -VGG16	CROP-DualGAN -VGG16
Cereal	0.947 ±0.011	0.955 ±0.008	0.965 ±0.008	0.960 ±0.016	0.962 ±0.009	0.960 ±0.009
Maize	0.970 ±0.017	0.970 ±0.028	0.977 ±0.013	0.982 ±0.011	0.981 ±0.023	0.983 ±0.007
Rape seed	0.873 ±0.044	0.900 ±0.041	0.929 ±0.019	0.919 ±0.034	0.918 ±0.025	0.926 ±0.022
Category	200			300		
	SSLAI	Random -SSLAI	CROP-DualGAN -SSLAI	SSLAI	Random -SSLAI	CROP-DualGAN -SSLAI
Cereal	0.962 ±0.018	0.960 ±0.017	0.973 ±0.008	0.964 ±0.017	0.969 ±0.011	0.976 ±0.012
Maize	0.912 ±0.066	0.945 ±0.060	0.961 ±0.021	0.940 ±0.042	0.949 ±0.033	0.976 ±0.008
Rape seed	0.893 ±0.049	0.922 ±0.026	0.940 ±0.011	0.904 ±0.038	0.928 ±0.036	0.943 ±0.010

Note: p is a value in Kruskal-Wallis H Test compared benchmark models with the proposed model, and significance level is 0.05.

TABLE VI
COMPARISON RESULTS OF THE RMSE IN THE BENCHMARK MODELS (MEAN ± STANDARD DEVIATION)

Category	200			300		
	VGG16	Random -VGG16	CROP-DualGAN -VGG16	VGG16	Random -VGG16	CROP-DualGAN -VGG16
Cereal	0.390 ±0.048	0.353 ±0.032	0.311 ±0.038	0.326 ±0.058	0.320 ±0.036	0.333 ±0.035
Maize	0.253 ±0.086	0.248 ±0.113	0.207 ±0.058	0.185 ±0.070	0.176 ±0.080	0.179 ±0.048
Rape seed	0.549 ±0.098	0.484 ±0.091	0.408 ±0.049	0.439 ±0.108	0.453 ±0.075	0.425 ±0.070
Category	200			300		
	SSLAI	Random -SSLAI	CROP-DualGAN -SSLAI	SSLAI	Random -SSLAI	CROP-DualGAN -SSLAI
Cereal	0.331 ±0.065	0.329 ±0.070	0.282 ±0.042	0.314 ±0.062	0.292 ±0.058	0.254 ±0.056
Maize	0.425 ±0.194	0.288 ±0.133	0.283 ±0.123	0.314 ±0.105	0.294 ±0.099	0.208 ±0.049
Rape seed	0.523 ±0.089	0.458 ±0.074	0.390 ±0.039	0.495 ±0.088	0.435 ±0.077	0.373 ±0.042

Note: p is a value in Kruskal-Wallis H Test compared benchmark models with the proposed model, and significance level is 0.05.

> REPLACE THIS LINE WITH YOUR MANUSCRIPT ID NUMBER (DOUBLE-CLICK HERE TO EDIT) <

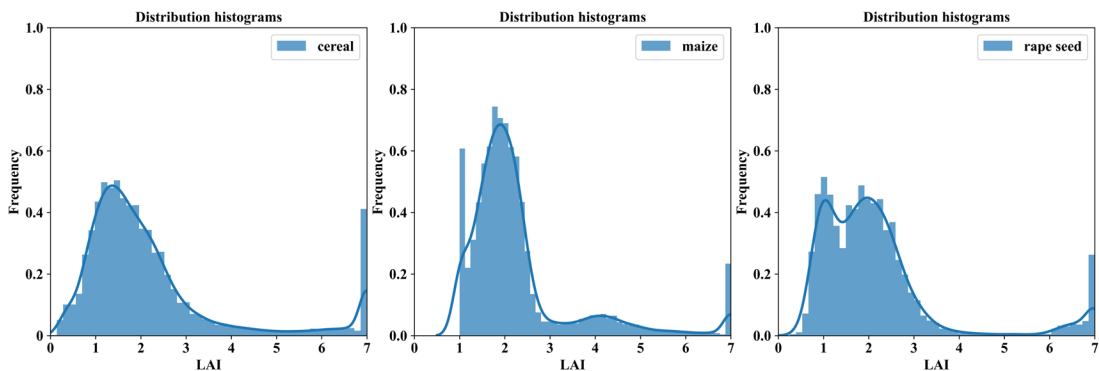


Fig. 4. Distribution for the LAI of cereal, maize and rape seed.

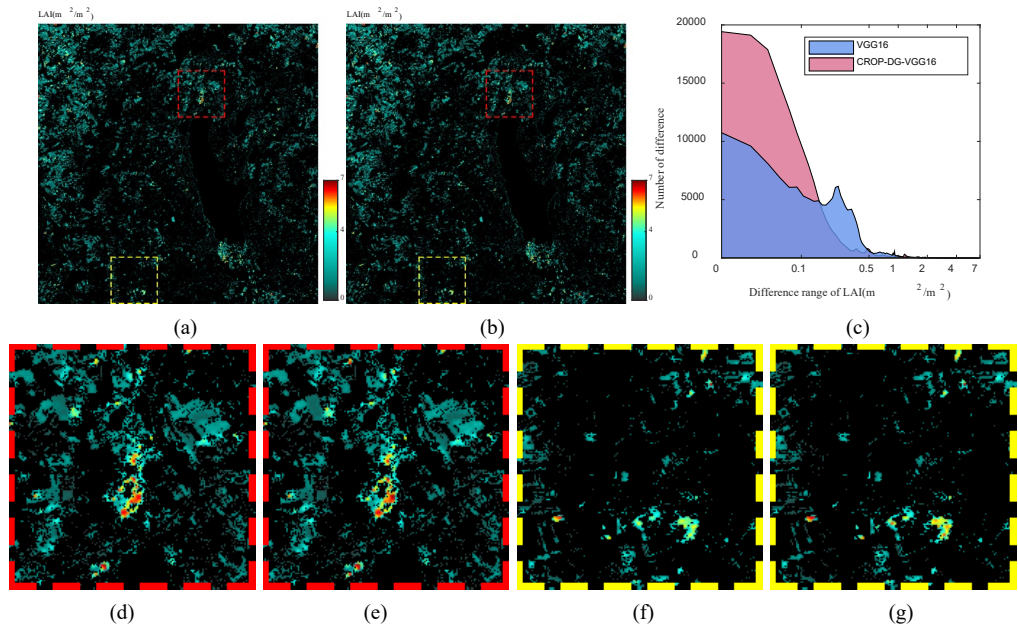


Fig. 5. Comparison of the LAI estimation of VGG16 based on 30 initial training samples and its enhancement. (a) and (b) are LAI estimation of VGG16 and CROP-DualGAN-VGG16, respectively. (c) is an error histogram, describing the comparison of above two models. It can be seen obviously that the error of CROP-DualGAN-VGG16 is smaller. (d) and (f) are details of VGG16. (e) and (g) are details of CROP-DualGAN-VGG16.

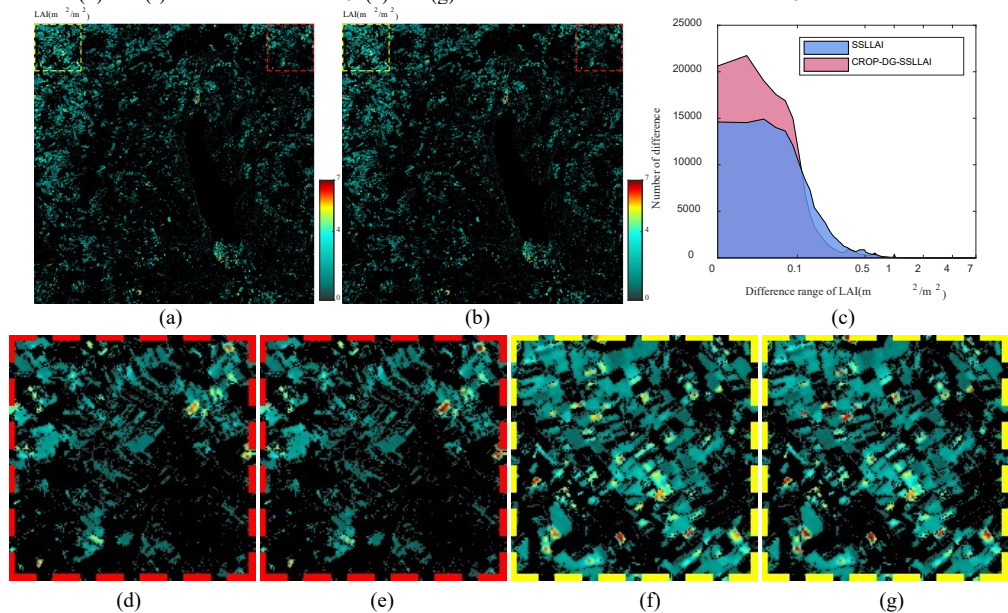


Fig. 6. Comparison of the LAI estimation of SSSLAI-Net based on 30 initial training samples and its enhancement. (a) and (b) are LAI estimation of SSSLAI-Net and CROP-DualGAN-SSLLAI-Net, respectively. (c) is an error histogram, describing the comparison of above two models. It can be seen obviously that the error of CROP-DualGAN-SSLLAI is smaller. (d) and (f) are details of SSSLAI-Net. (e) and (g) are details of CROP-DualGAN-SSLLAI-Net.

> REPLACE THIS LINE WITH YOUR MANUSCRIPT ID NUMBER (DOUBLE-CLICK HERE TO EDIT) <

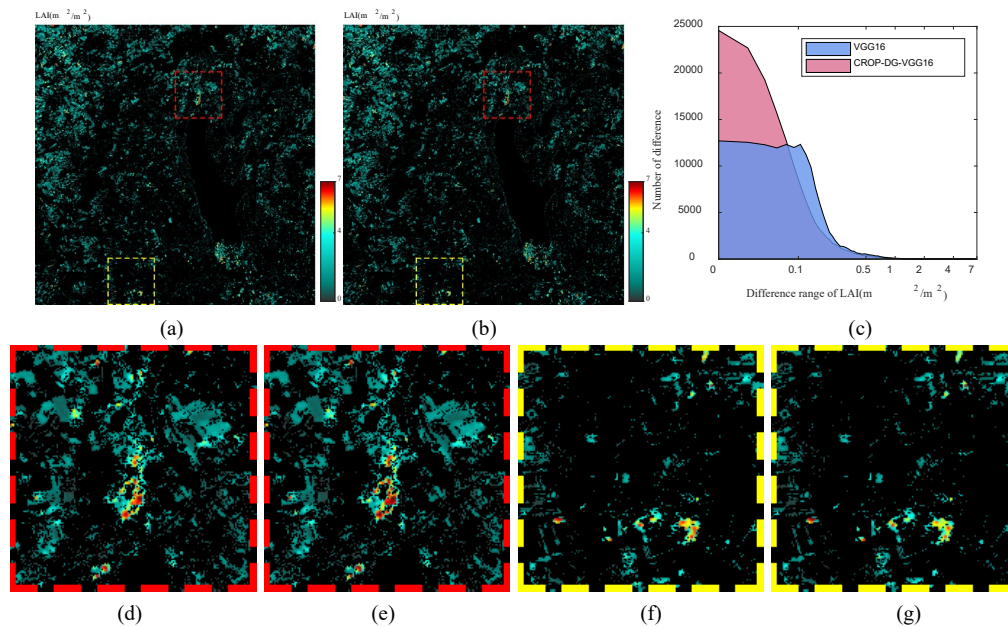


Fig. 7. Comparison of the LAI estimation of VGG16 based on 200 initial training samples and its enhancement. (a) and (b) are LAI estimation of VGG16 and CROP-DualGAN-VGG16, respectively. (c) is an error histogram, describing the comparison of above two models. It can be seen obviously that the error of CROP-DualGAN-VGG16 is smaller. (d) and (f) are details of VGG16. (e) and (g) are details of CROP-DualGAN-VGG16.

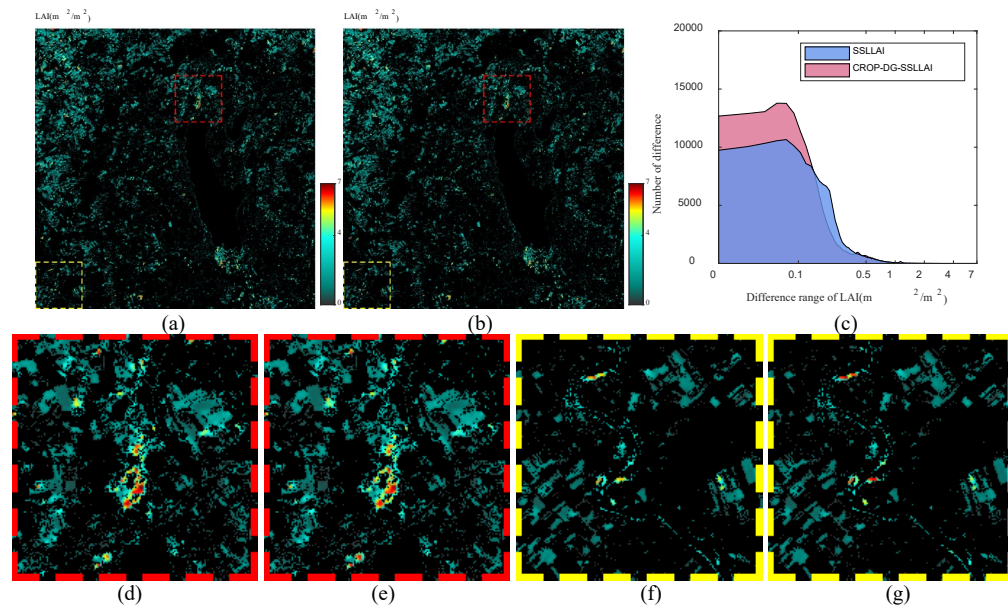
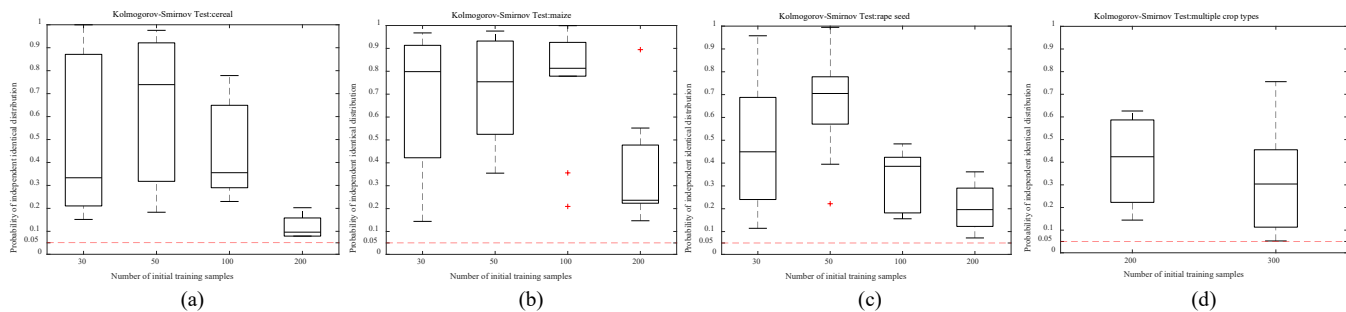


Fig. 8. Comparison of the LAI estimation results of SSSLAI-Net based on 200 initial training samples and its enhancement. (a) and (b) are LAI estimation of SSSLAI-Net and CROP-DualGAN-SSLLAI-Net, respectively. (c) is an error histogram, describing the comparison of above two models. It can be seen obviously that the error of CROP-DualGAN-SSLLAI is smaller. (d) and (f) are details of SSSLAI-Net. (e) and (g) are details of CROP-DualGAN-SSLLAI-Net.



> REPLACE THIS LINE WITH YOUR MANUSCRIPT ID NUMBER (DOUBLE-CLICK HERE TO EDIT) <

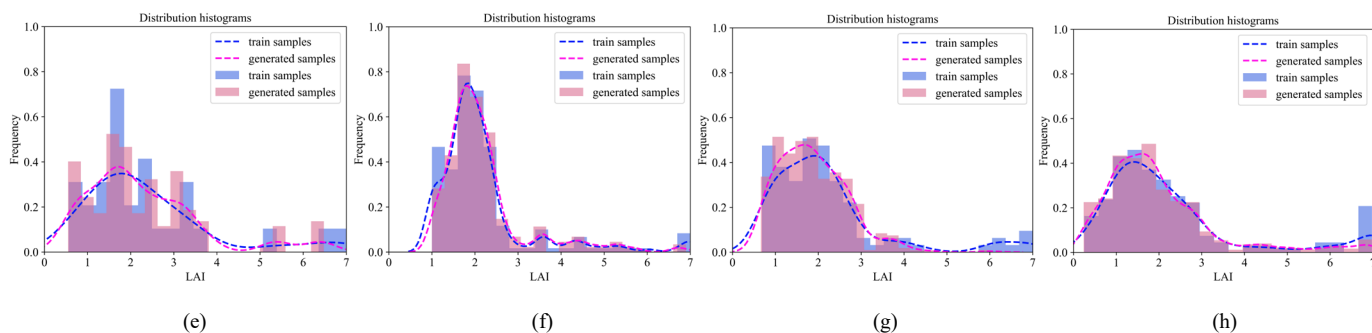


Fig. 9. The Kolmogorov-Smirnov results of single crop type experiments and multiple crop types experiments. (a), (b), and (c) represent the significance results in cereal, maize and rape seed experiments, separately. (d) represents the significance results in multiple crop types experiments. (e), (f), (g), and (h) are the examples of the distribution of initial training samples and its generated, separately.

IV. Conclusion

Currently, the problem to estimate LAI with deep learning is that measured samples is insufficient, while the CROP-DualGAN proposed in this paper can solve the above problem through data enhancement. Experiments prove that most of the samples enhanced by CROP-DualGAN is effective on LAI estimation improvement. The proposed method is universal to solve insufficient samples. However, in the multiple crop types experiments, the accuracy of LAI estimation is obviously lower than that of single crop type experiments. In the next work, we will focus on solving data imbalance to improve LAI estimation in the multiple crop types experiments. Data enhancement for small samples to improve LAI estimation can be applied to further support crop growth condition monitoring, crop stresses (drought, flood, pest, disease, etc.) detection, and yield estimation. Moreover, LAI has an important role in the calculation of ecosystem carbon sink, so this data enhancement method and algorithm can be extended to the crop, forest, grass etc. vegetation parameter estimation to support the research in the future.

ACKNOWLEDGMENTS

The authors would like to thank European Space Agency for providing the EnMAP datasets.

REFERENCES

- [1] J. M. Chen, T. A. Black, "Defining leaf area index for non-flat leaves," *Plant Cell Environment*, vol. 15, no. 4, pp. 421-429, 1992. DOI: 10.1111/j.1365-3040.1992.tb00992.x.
- [2] Y. Liu, R. Liu, and J. M. Chen, "Retrospective retrieval of long-term consistent global leaf area index (1981–2011) from combined AVHRR and MODIS data," *Journal of Geophysical Research: Biogeosciences*, vol. 117, no. G4, 2012. DOI: 10.1029/2012JG002084.
- [3] R. B. Myneni, S. Hoffman, Y. Knyazikhin, *et al.*, "Global products of vegetation leaf area and fraction absorbed PAR from year one of MODIS data," *Remote sensing of environment*, vol. 83, no. 1-2, pp. 214-231, 2002. DOI: 10.1016/S0034-4257(02)00074-3.
- [4] X. Zhou, H. B. Zheng, X. Q. Xu, *et al.*, "Predicting grain yield in rice using multi-temporal vegetation indices from UAV-based multispectral and digital imagery," *ISPRS Journal of Photogrammetry and Remote Sensing*, vol. 130, pp. 246-255, 2017.
- [5] H. Zhou, C. Wang, G. Zhang, *et al.*, "Generating a spatio-temporal complete 30 m leaf area index from field and remote sensing data," *Remote Sensing*, vol. 12, no. 15, pp. 2394, 2020.
- [6] G. Omer, O. Mutanga, E. Abdel-Rahman and E. Adam, "Empirical prediction of leaf area index (LAI) of endangered tree species in intact and fragmented indigenous forests ecosystems using WorldView-2 data and two robust machine learning algorithms," *Remote Sensing*, vol. 8, no. 4, pp. 324, 2016. DOI: 10.3390/rs8040324.
- [7] G. Zheng, and L. M. Moskal, "Retrieving leaf area index (LAI) using remote sensing: theories, methods and sensors," *Sensors*, vol. 9, no. 4, pp. 2719-2745, 2009. DOI: 10.3390/s90402719.
- [8] K. Yan, T. Park, G. Yan, *et al.*, "Evaluation of MODIS LAI/FPAR product collection 6. Part 2: Validation and intercomparison," *Remote Sensing*, vol. 8, no. 6, pp. 460, 2016. DOI: 10.3390/rs8060460.
- [9] H. Fang, F. Baret, S. Plummer and G. Schaepman-Strub, "An Overview of Global Leaf Area Index (LAI): Methods, Products, Validation, and Applications," *Reviews of Geophysics*, vol. 57, no. 3, pp. 739-799, 2014. DOI: 10.1029/2018RG000608.
- [10] K. S. Lee, W. B. Cohen, R. E. Kennedy, T. K. Maitersperger and S. T. Gower, "Hyperspectral versus multispectral data for estimating leaf area index in four different biomes," *Remote Sensing of Environment*, vol. 91, no. 3-4, pp. 508-520, 2004. DOI: 10.1016/j.rse.2004.04.010.
- [11] Y. Sun, Q. Qin, H. Ren, T. Zhang and S. Chen, "Red-edge band vegetation indices for leaf area index estimation from Sentinel-2/MSI imagery," *IEEE Transactions on Geoscience and Remote Sensing*, vol. 58, no. 2, pp. 826-840, 2019. DOI: 10.1109/TGRS.2019.2940826.
- [12] M. Maki, and K. Homma, "Empirical regression models for estimating multiyear leaf area index of rice from several vegetation indices at the field scale," *Remote Sensing*, vol. 6, no. 6, pp. 4764-4779, 2014. DOI: 10.3390/rs6064764.
- [13] Y. Zhang, J. Yang, X. Liu, L. Du, S. Shi, J. Sun and B. Chen, "Estimation of Multi-Species Leaf Area Index Based on Chinese GF-1 Satellite Data Using Look-Up Table and Gaussian Process Regression Methods," *Sensors*, vol. 20, no. 9, pp. 1-15, 2020. DOI: 10.3390/s20092460.
- [14] K. Liu, Q. Zhou, W. Wu, T. Xia and H. Tang, "Estimating the crop leaf area index using hyperspectral remote sensing," *Journal of integrative agriculture*, vol. 15, no. 2, pp. 475-491, 2016. DOI: 10.1016/S2095-3119(15)61073-5.
- [15] L. Wang, Q. Chang, J. Yang, X. Zhang, F. Li and Y. Xu, "Estimation of paddy rice leaf area index using machine learning methods based on hyperspectral data from multi-year experiments," *PLoS ONE*, vol. 13, no. 12, 2018. DOI: 10.1371/journal.pone.0207624.
- [16] B. Sun, C. Wang, C. Yang, B. Xu and J. Zhang, "Retrieval of rapeseed leaf area index using the PROSAIL model with canopy coverage derived from UAV images as a correction parameter," *International Journal of Applied Earth Observation and Geoinformation*, vol. 102, 2021. DOI: 10.1016/j.jag.2021.102373.
- [17] X. Jin, L. Kumar, Z. Li, H. Feng, X. Xu, G. Yang and J. Wang, "A review of data assimilation of remote sensing and crop models," *European Journal of Agronomy*, vol. 92, pp. 141-152, 2018.
- [18] X. Zhan, Z. Xiao, J. Jiang and H. Shi, "A data assimilation method for simultaneously estimating the multiscale leaf area index from time-series multi-resolution satellite observations," *IEEE Transactions on Geoscience and Remote Sensing*, vol. 57, no. 11, pp. 9344-9361, 2019. DOI: 10.1109/TGRS.2019.2926392.
- [19] R. Srinet, S. Nandy, and N. R. Patel, "Estimating leaf area index and light extinction coefficient using Random Forest regression algorithm in a tropical moist deciduous forest, India," *Ecological Informatics*, vol. 52, pp. 94-102, 2019. DOI: 10.1016/j.ecoinf.2019.05.008.
- [20] L. Sun, W. Wang, C. Jia and X. Liu, "Leaf area index remote sensing based on Deep Belief Network supported by simulation data," *International Journal of Remote Sensing*, vol. 42, no. 20, pp. 7637-7661,

> REPLACE THIS LINE WITH YOUR MANUSCRIPT ID NUMBER (DOUBLE-CLICK HERE TO EDIT) <

2021. DOI: 10.1080/01431161.2021.1942584.

[21] M. Hosseini, H. McNairn, S. Mitchell, A. Davidson and L. D. Robertson, "Comparison of machine learning algorithms and water cloud model for leaf area index estimation over corn fields." *IGARSS 2019 - 2019 IEEE International Geoscience and Remote Sensing Symposium IEEE*, pp. 6267-6270, 2019. DOI: 10.1109/IGARSS.2019.8900445.

[22] Z. Xiao, S. Liang, J. Wang, Y. Xiang, X. Zhao and J. Song, "Long-time-series global land surface satellite leaf area index product derived from MODIS and AVHRR surface reflectance," *IEEE Transactions on Geoscience and Remote Sensing*, vol. 54, no. 9, pp. 5301-5318, 2016. DOI: 10.1109/TGRS.2016.2560522.

[23] Y. Huanhuan, Y. Guijun, L. Changchun, *et al.*, "Retrieving Soybean Leaf Area Index from Unmanned Aerial Vehicle Hyperspectral Remote Sensing: Analysis of RF, ANN, and SVM Regression Models," *Remote Sensing*, vol. 9, no. 4, pp. 309, 2017. DOI: 10.3390/rs9040309.

[24] X. Xu, J. Lu, N. Zhang, *et al.*, "Estimation of rice canopy chlorophyll content and leaf area index based on coupling of radiative transfer and Bayesian network models," *ISPRS Journal of Photogrammetry and Remote Sensing*, vol. 150, pp. 185-196, 2019.

[25] X. Quan, B. He, X. Li, "A Bayesian network-based method to alleviate the ill-posed inverse problem: A case study on leaf area index and canopy water content retrieval," *IEEE Transactions on Geoscience & Remote Sensing*, vol. 53, no. 12, pp. 6507-6517, 2015.

[26] S. C. Smid, D. McNeish, M. Miočević, *et al.* "Bayesian versus frequentist estimation for structural equation models in small sample contexts: A systematic review". *Structural Equation Modeling: A Multidisciplinary Journal*, vol. 27, no. 1, pp. 131-161, 2020.

[27] X. Li, Y. Dong, Y. Zhu and W. Huang, "Leaf area index estimation with EnMAP hyperspectral data based on deep neural network," *Journal of Infrared and Millimeter Waves*, vol. 39, no. 1, pp. 111-119, 2020.

[28] W. Gan, P. K. Wong, G. Yu, *et al.* "Light-weight network for real-time adaptive stereo depth estimation". *Neurocomputing*, vol. 441, pp. 118-127, 2021.

[29] D. Feng, H. Chen. "A small samples training framework for deep Learning-based automatic information extraction: Case study of construction accident news reports analysis". *Advanced Engineering Informatics*, vol. 47, pp. 101256-101268, 2021.

[30] B. Cai, C. Sheng, C. Gao, *et al.* "Artificial intelligence enhanced reliability assessment methodology with small samples". *IEEE Transactions on Neural Networks and Learning Systems*, 2021.

[31] P. Isola, J. Y. Zhu, T. Zhou and A. Efros, "Image-to-image translation with conditional adversarial networks." *Proceedings of the IEEE conference on computer vision and pattern recognition*, pp. 1125-1134, 2017.

[32] Z. Yi, H. Zhang, P. Tan and M. Gong, "Dualgan: Unsupervised dual learning for image-to-image translation." *IEEE Computer Society*, pp. 2849-2857, 2017.

[33] X. Qu, X. Wang, Z. Wang, Z. Wang, L. Wang and L. Zhang, "Perceptual-DualGAN: perceptual losses for image to image translation with generative adversarial nets." *2018 International Joint Conference on Neural Networks (IJCNN)*, pp. 1-8, 2018.

[34] M. Omdal, "Final: CycleGAN and DualGAN on Artistic Image-to-Image Translation," 2019.

[35] Z. Li, C. Sun, C. Liu, X. Chen, M. Wang and Y. Liu, "RCC-Dual-GAN: An Efficient Approach for Outlier Detection with Few Identified Anomalies," 2020. DOI: 10.48550/arXiv.2003.03609.

[36] D. Prokopenko, J. V. Stadelmann, H. Schulz, S. Renisch and D. V. Dylov, "Synthetic CT Generation from MRI Using Improved DualGAN," 2019.

[37] A. Aggarwal, M. Mittal and G. Battineni, "Generative adversarial network: An overview of theory and applications." *International Journal of Information Management Data Insights*, vol. 1, no. 1, 2021. DOI: 10.1016/j.jjime.2020.100004.

[38] H. Alqahtani, M. Kavakli and G. Kumar, "Applications of Generative Adversarial Networks (GANs): An Updated Review." *Archives of Computational Methods in Engineering*, vol. 28, no. 2, pp. 525-552, 2019. DOI: 10.1016/j.jjime.2020.100004.

[39] O. Ronneberger, P. Fischer, and T. Brox, "U-net: Convolutional networks for biomedical image segmentation." *International Conference on Medical image computing and computer-assisted intervention*, pp. 234-241, 2015.

[40] I. Gulrajani, F. Ahmed, M. Arjovsky, V. Dumoulin and A. C. Courville, "Improved training of wasserstein gans," *Advances in neural information processing systems*, vol. 30, 2017.

[41] Y. Hong, U. Hwang, J. Yoo and S. Yoon, "How Generative Adversarial

Nets and its variants Work: An Overview of GAN," *ACM Computing Surveys*, vol. 52, no. 1, 2017. DOI: 10.1145/3301282.

[42] M. Arjovsky and L. Bottou, "Towards principled methods for training generative adversarial networks," 2017. arXiv preprint arXiv:1701.04862.

[43] M. Arjovsky, S. Chintala, and L. Bottou, "Wasserstein GAN," 2017. arXiv preprint arXiv:1701.07875.

[44] E. Z. Ramos, M. Nakakuni, and E. Yfantis, "Quantitative measures to evaluate neural network weight initialization strategies." 2017 IEEE 7th Annual Computing and Communication Workshop and Conference (CCWC). IEEE, pp. 1-7, 2017.

[45] S. Migdall, H. Bach, and H. Kaufmann, "Simulation of EnMAP-like hyperspectral images based on textural information and a radiative transfer approach," *Proceedings of the Hyperspectral Workshop, Frascati, Italy*, pp. 17-19, 2010.

[46] W. Verhoef and H. Bach, "Coupled soil-leaf-canopy and atmosphere radiative transfer modeling to simulate hyperspectral multi-angular surface reflectance and TOA radiance data," *Remote Sensing of Environment*, vol. 109, no. 2, pp. 166-182, 2007.

[47] K. Simonyan and A. Zisserman, "Very deep convolutional networks for large-scale image recognition," *Computer Science*, 2014. arXiv preprint arXiv:1409.1556.



remote sensing.

Xueling Li received the B.S. degree in information and computing science from Qilu University of Technology, Shandong, China, in 2017, and the M.S. degree in mathematics of computation from Capital Normal University, Beijing, China, in 2020. Her research interests include research and application in vegetation



Yingying Dong received the B.S. degree in information and computation science from Shandong Normal University, Shandong, China, in 2006, the M.S. degree in mathematics of computation from Capital Normal University, Beijing, China, in 2009, and the Ph.D. degree in agricultural remote sensing and information technology from Zhejiang University, Zhejiang, China, in 2013. Her research interests include research and application in vegetation remote sensing.



Yining Zhu received the B.S. degree in information and scientific computing from Beijing Information and Technology Institute in 2006, the M.S and the Ph.D degree in mathematics and information technology from Capital Normal University, Beijing, China, in 2009 and 2012, respectively. He was a Postdoc at the Peking University, Beijing, China, from 2013 to 2014. He is an associate professor in the school of mathematical science at Capital Normal University. His current research interests include image reconstruction, deep learning-based artifact correction and image processing.

> REPLACE THIS LINE WITH YOUR MANUSCRIPT ID NUMBER (DOUBLE-CLICK HERE TO EDIT) <



Wenjiang Huang received the Ph.D. degree in cartography and GIS from Beijing Normal University, Beijing, China, in 2005. Currently, he is a Professor with the Key Laboratory of Digital Earth Science, Aerospace Information Research Institute, Chinese Academy of Sciences, Beijing, China. His research interests include

quantitative remote sensing research and application in vegetation.